Applied Catalysis B: Environmental 200 (2017) 566–577

Contents lists available at ScienceDirect

Applied Catalysis B: Environmental

journal homepage: www.elsevier.com/locate/apcatb

Carbon dioxide reforming of methane over Ru catalysts supported on Mg-Al oxides: A highly dispersed and stable Ru/Mg(Al)O catalyst

Dalin Li, Rule Li, Miaomiao Lu, Xingyi Lin, Yingying Zhan, Lilong Jiang*

National Engineering Research Center of Chemical Fertilizer Catalyst (NERC-CFC), School of Chemical Engineering, Fuzhou University, Gongye Road No.523, Fuzhou 350002, Fujian, PR China

ARTICLE INFO

Article history:
Received 13 May 2016
Received in revised form 11 July 2016
Accepted 28 July 2016
Available online 28 July 2016

Keywords:
Methane carbon dioxide reforming
Ruthenium catalyst
Layered double hydroxides
Magnesium-aluminum mixed metal oxide
Memory effect

ABSTRACT

Ru catalysts (2 wt%) supported on Mg and/or Al oxides including γ-Al_2O_3, $MgAl_2O_4$, Mg_3(Al)O, and MgO were prepared by incipient wetness impregnation and compared for the CH_4-CO_2 reforming to investigate the effect of support on the Ru dispersion and catalytic performance. The catalysts before and after reaction were well characterized by using N_2 physical adsorption, ICP, SEM-EDX, XRD, H_2-TPR, TEM, CO chemisorption, FTIR of CO adsorption, XPS, CO_2-TPD, TG, and Raman spectroscopy. The characterization results revealed that Ru metal was very highly dispersed on the Mg_3(Al)O mixed oxide obtained from Mg-Al layered double hydroxide, probably existing in very small nanoparticles and/or clusters. The order of Ru metal dispersion was Ru/Mg_3(Al)O > Ru/MgO > Ru/$MgAl_2O_4$ > Ru/γ-Al_2O_3. The catalytic activity and stability of the Ru catalysts were greatly dependent on the support. Both Ru/MgO and Ru/Mg_3(Al)O showed higher activity than Ru/$MgAl_2O_4$ and Ru/γ-Al_2O_3, which might be related to the strong base intensity of support and more accessible surface Ru^0 atoms, respectively. During 30 h of reaction at 1023 K, a significant deactivation occurred on Ru/γ-Al_2O_3, Ru/$MgAl_2O_4$, and Ru/MgO, which was mainly attributed to the sintering of Ru metal particles. In contrast, the Ru/Mg_3(Al)O catalyst exhibited superior stability and no significant sintering of Ru metal was observed, suggesting that the highly dispersed Ru metal was stable. A 300 h long-term test further demonstrated the excellent stability of Ru/Mg_3(Al)O. These results highlight the significant effect of Mg(Al)O mixed oxide on the improvement of Ru dispersion and catalytic performance, and this might be related to the unique properties of Mg(Al)O mixed oxide including memory effect, low crystallinity, and its strong interaction with Ru.

1. Introduction

Carbon dioxide reforming of methane to synthesis gas is a very attractive route for the production of energy and chemicals [1–3]. The great advantages of this reaction involve the use of two greenhouse gases, which are also two of the most abundant carbon-containing materials, and the formation of synthesis gas that is an important feedstock for Fischer-Tropsch synthesis and methanol synthesis. Most of the Group VIII metals are reported to be more or less catalytically active towards this reaction. However under the reforming conditions, the catalyst may suffer from rapid deactivation due to coke deposition and/or sintering of metal particles. Therefore, it is highly desired to develop a thermally stable catalyst that will resist coke deposition and sintering. Non-noble metal nickel has been extensively investigated because of its low cost, wide availability, and relatively high activity [2,4]. Nevertheless, the major problem of Ni catalyst is the serious coke deposition, and the development of a coke-resistant Ni catalyst still remains a great challenge. On the other hand, noble metals such as Ru and Rh are showed to be more active and more resistant to coke deposition as compared to non-noble metals. In particular, several studies have reported that Ru supported on Al_2O_3 [5], MgO [6], and TiO_2 [7] showed superior activity than other supported Group VIII metals. Considering the high activity of Ru and its low cost compared with other noble metals, Ru catalyst could be a potential choice for the CH_4-CO_2 reforming.

Various supports including Al_2O_3 [8–11], TiO_2 [12], CeO_2 [13], ZrO_2 [10], CeO_2-ZrO_2 [14], La_2O_3 [15], pyrochlore [16], zeolites [17], carbon [9,11], and their composites [8,18] have been used to prepare Ru catalyst for the CH_4-CO_2 reforming. Solymosi et al. [5] reported that the specific activity of alumina supported noble-metal catalysts decreased in the order of Ru > Pd > Rh > Pt > Ir, which agreed with their activity order towards the dissociation of CO_2. Ferreira-Aparicio et al. [9] have proposed a bifunctional mechanism

* Corresponding author.
E-mail address: jll@fzu.edu.cn (L. Jiang).

http://dx.doi.org/10.1016/j.apcatb.2016.07.050
0926-3373/

for Ru/Al_2O_3, in which the hydroxyl groups of the Al_2O_3 support may activate CO_2 by producing carbonate and/or bicarbonate that further transform to formate intermediates and subsequently decompose releasing CO. MgO is also an effective support for Ru reforming catalyst. Rostrup-Nielsen and Hansen [6] compared the CH_4-CO_2 reforming over MgO supported transition metals and found that the activity decreased in the order Ru > Rh, Ni > Ir, Pt, Pd and that Ru showed high selectivity for carbon-free operation. It is suggested that the presence of MgO would increase the basicity of the catalyst and increase the surface coverage with hydroxyls via reverse water gas shift reaction, which is beneficial for carbon gasification. The good performance of Ru catalysts supported on Al_2O_3 and MgO induces our great interest to use Mg-Al mixed oxides as catalyst support, e.g., $MgAl_2O_4$ spinel and Mg(Al)O solid solution. Mg(Al)O solid solution, where Al^{3+} ions are incorporated into the MgO framework, can be obtained from Mg-Al layered double hydroxides (LDHs). LDHs are a class of two-dimensional anionic clays consisting of positively charged brucite-like layers and exchangeable interlayer anions, and they produce mixed oxides by heating that show interesting properties such as high surface area, basic properties, thermal stability, and "memory effect" [19]. As reported [20], the LDHs-derived Mg(Al)O solid solution shows much higher surface area than MgO, which would be favorable for the metal dispersion. On the other hand, Mg(Al)O is expected to process more basic sites than Al_2O_3 due to the basic property of MgO, which may benefit the CO_2 adsorption and activation. The advantages of Mg(Al)O compared to MgO and Al_2O_3 make it a promising catalyst support for hydrocarbon reforming. Actually, the LDHs-derived Mg(Al)O-supported Ni-based catalysts have been reported to perform well in catalytic reforming of CH_4 [21–23] and biomass tar [24–26]. Nevertheless, as far as we known, there are very few reports on the preparation of Mg(Al)O supported Ru catalyst [27] and its application in the CH_4-CO_2 reforming [28].

In the present work, a comparative investigation of CH_4-CO_2 reforming over Ru catalysts supported on Mg and/or Al oxides including γ-Al_2O_3 $MgAl_2O_4$, Mg_3(Al)O, and MgO was undertaken. The effect of support on the Ru metal dispersion and catalytic activity and stability for the CH_4-CO_2 reforming was investigated. Ru supported catalysts (2 wt%) were prepared by impregnation method and tested for the CH_4-CO_2 reforming at 873–1073 K. The catalysts before and after reaction were characterized by various techniques including N_2 physical adsorption, inductive coupled plasma (ICP), scanning electron microscopy-energy dispersive X ray (SEM-EDX), X-ray diffraction (XRD), temperature-programmed reduction with H_2 (H_2-TPR), temperature-programmed desorption of CO_2 (CO_2-TPD), Fourier transform infrared spectroscopy of CO adsorption (CO-FTIR), CO chemisorption, transmission electron microscope (TEM), X-ray photoelectron spectroscopy (XPS), thermogravimetric analysis (TG), and Raman spectroscopy, to reveal the structure-performance relationship. It is found that the Ru metal supported on the Mg_3(Al)O mixed oxide was very highly dispersed and exhibited superior catalytic stability for the CH_4-CO_2 reforming, highlighting the significant effect of Mg(Al)O support on the improvement of Ru dispersion and catalytic performance.

2. Experimental

2.1. Catalyst preparation

The supports, i.e., γ-Al_2O_3, $MgAl_2O_4$, Mg_3(Al)O, and MgO were synthesized by co-precipitation method. Particularly, the Mg_3(Al)O support was obtained by the thermal decomposition of Mg_3Al LDH. In this case, a mixed aqueous solution of $Mg(NO_3)_2{\cdot}6H_2O$ and $Al(NO_3)_3{\cdot}9H_2O$ was dropwise added to an aqueous solution of Na_2CO_3 under stirring, during which the pH value of the solution was adjusted to 10 ± 0.5 with 2 M NaOH aqueous solution. The molar ratio of Mg^{2+}: Al^{3+}: CO_3^{2-} was 3:1:0.5 according to the formula of hydrotalcite $[Mg_6Al_2(OH)_{16}]CO_3{\cdot}4H_2O$. The precipitate was filtered and washed with de-ionized water several times to remove Na^+ ions. The obtained powder was dried at 373 K for 24 h and calcined in air at 1073 K for 5 h. Other supports, i.e., $MgAl_2O_4$, γ-Al_2O_3, and MgO were synthesized by a similar procedure as described above, whereas in the cases of γ-Al_2O_3 and MgO the Na_2CO_3 solution was replaced with de-ionized water. The BET surface areas of the obtained γ-Al_2O_3, $MgAl_2O_4$, Mg_3(Al)O, and MgO supports are 131, 108, 164, and 20 $m^2\ g^{-1}$, respectively.

Ru supported catalysts were prepared by incipient wet impregnation method. Typically, an aqueous solution of ruthenium chloride ($RuCl_3{\cdot}nH_2O$) was dropwise added to the support, followed by drying at 373 K for 24 h and calcination at 773 K for 5 h under air atmosphere. The sample was pressed, crushed and sieved to particle sizes of 30–60 mesh. The nominal Ru loading was 2 wt%.

2.2. Catalyst characterization

The Ru loading in each sample was measured by inductively coupled plasma (ICP) on OPTIMA 8000 (PerkinElmer) after the sample was completely dissolved using nitro-hydrochloric acid. N_2 physical adsorption was conducted at 77 K on a Micromeritics ASAP 2020 instrument. Before N_2 adsorption, the sample was pretreated at 453 K for 4 h in vacuum and the surface area was calculated by the Brunauer-Emmett-Teller (BET) method. The powder X-ray diffraction (XRD) patterns were recorded by a PANalytical X'pert Pro diffractometer with Co Kα ($\lambda = 0.1789$ nm) radiation operating at 40 kV and 40 mA. Scanning electron microscopy and energy dispersive X-ray (SEM-EDX) measurements were conducted on Hitachi-S4800 equipment operated at 5.0 kV. Transmission electron microscope (TEM) photographs were taken by means of TECNAI G2F20 equipment operated at 200 kV. The catalysts were crushed to fine powders, dispersed in ethanol by supersonic waves, and then deposited on a Cu grid with a holey carbon film. The particle size was estimated by $\Sigma n_i d_i^3 / \Sigma n_i d_i^2$, where d_i is the diameter of particles and n_i is the number of particles with diameter d_i.

Temperature-programmed reduction with H_2 (H_2-TPR) and temperature-programmed desorption of CO_2 (CO_2-TPD) were carried out on an AutoChem 2920 apparatus equipped with a thermal conductivity detector (TCD). For H_2-TPR, 100 mg of sample was purged with Ar gas at 573 K for 0.5 h, and cooled down to ambient temperature under the same gas flow, finally the sample was reduced with 10% H_2/Ar (30 mL min^{-1}) from ambient temperature to 873 K at a heating rate of 10 K min^{-1}. For CO_2-TPD, the sample was pre-reduced with H_2 at 873 K for 0.5 h, and the CO_2 adsorption was carried out at 323 K for 1 h. TPD was performed in Ar flow by raising the temperature from 323 to 1173 K.

CO chemisorption was conducted on AutoChem 2920 at ambient temperature with 5% CO/He gas stream. 100 mg of sample was firstly reduced with H_2 at 873 K for 0.5 h, then purged with He to remove the remaining gas and cooled down to ambient temperature under the same gas flow. The CO consumption was monitored by TCD. Uptake of CO at monolayer coverage of Ru species was used to estimate Ru metal dispersion and particle size. Dispersion (%) = (CO absorption)/(H_2 consumption in TPR/2) × 100%. The particles size of Ru metal was calculated by the equation: d (nm) = $(6 \times \nu_m)/(D \times a_m)$, where D is the metal dispersion, ν_m is the volume occupied by a metal atom in the bulk (13.65×10^{-3} nm^3), and a_m is the surface area occupied by an exposed surface metal atom (9.09×10^{-2} nm^2) [29].

Diffuse reflectance infrared Fourier transform spectroscopy of CO adsorption (CO-FTIR) was conducted on a Perkin-Elmer IR spectrometer using an IR cell with ZnSe windows. The finely ground pre-reduced sample was placed in a sample holder and was in situ

treated in the DRIFT cell with H_2 at 873 K for 0.5 h. After reduction treatment, the temperature was further held at 873 K for 0.5 h and the sample was purged with high-purity He. When the sample was cooled to ambient temperature under the He flow, a reference spectrum was taken. Then a 5% CO/He flow was introduced to the sample for 0.5 h, and after purging with He, the spectrum was recorded. The IR spectrum of adsorbed CO was obtained by subtracting the reference spectrum.

X-ray photoelectron spectroscopy (XPS) was performed on an ESCALAB 250 spectrometer (Thermo Scientific) using Al Kα radiation (1486.8 eV) generated at 120 W. All binding energies were calibrated with respect to the C1 s peak (284.6 eV) arising from adventitious carbon. Raman spectroscopy was measured at ambient temperature using a Renishaw inVia Reflex Raman spectrometer with a 532 nm Ar ion laser as the excitation source. Thermogravimetric analysis (TG) was performed with a Perkin Elmer TG analyzer (TG-7) over ~5 mg of sample under an air flow (20 mL min^{-1}) from ambient temperature to 1073 K at a heating rate of 10 K min^{-1}.

2.3. Catalytic reaction

The catalytic performance for the CH_4-CO_2 reforming was tested in a fixed-bed quartz reactor under atmosphere pressure. Typically, about 50 mg of catalyst was pre-reduced with H_2 at 873 K for 0.5 h, then the reactant gas (CH_4:CO_2:N_2 = 1:1:2) was introduced into the reactor when the desired temperature was reached. The flow rate of the reactant gas was 50 mL min^{-1}, corresponding to a space velocity of 60,000 mL g^{-1} h^{-1}. The product gas was analyzed by an online gas chromatograph (GC-2014, Shimadzu) equipped with a TCD and a 13X molecular sieve column. For activity tests, the reaction temperature was increased step by step from 873 K to 1073 K; at each temperature, the activity was evaluated for 1 h. For stability tests, the reaction was conducted at 1023 K for 30 h. After the reaction, the reactant gas was stopped and the catalyst was cooled down to ambient temperature and then taken out of the reactor for further characterization. A 300 h of long-term stability test was further carried out on the best Ru/Mg_3(Al)O catalyst. In each test, the carbon balance of product gas (CH_4, CO_2, and CO) with respect to the fed gas was 100 ± 1%. The coke deposition was quite small and negligible as compared to the carbon-containing gaseous products.

3. Results and discussion

3.1. Structural and physicochemical properties of the Ru catalysts

Table 1 shows the actual Ru loadings of the calcined samples determined by ICP analysis. The Ru loading of the Ru/γ-Al_2O_3, Ru/$MgAl_2O_4$, and Ru/Mg_3(Al)O samples was similar to the nominal value (2 wt% or 0.20 mmol g_{cat}^{-1}), while the Ru/MgO sample showed a lower Ru loading than the nominal one. To check the reason, the Ru loading after impregnation of $RuCl_3$ with MgO was analyzed by ICP, which showed a value of 1.9 wt% with respect to MgO, suggesting that most of the Ru precursor was loaded on the MgO support. It could thus be inferred that some Ru precursor was lost during the calcination. This was probably due to the Ru volatilization by the formation of RuO_4 ($RuO_2(s) + O_2(g) \rightarrow RuO_4(g)$ [30]). The chemical compositions of the calcined samples were also analyzed by SEM-EDX (Supplementary material, Fig. S1 and Tables S1). The Ru loading determined by EDX was somewhat different with that measured by ICP, which was properly caused by the limitation of each method. The presence of a small amount of residual Na (<1.1 wt%) and Cl (<0.33 wt%) species were also detected by EDX. The Cl/Ru molar ratios (0.12–0.17) determined from EDX were much lower than ratio of 3 present in the Ru salt precursor, illus-

Table 1
Physicochemical properties of the Ru supported catalysts before and after reaction.

Catalyst	Before reaction							After reaction				
	Ru loading[a] (mmol g^{-1}_{cat})	BET surface area[b] (m^2 g^{-1}_{cat})	H_2 consumption[c] (mmol g^{-1}_{cat})	CO adsorption[d] (μmol g^{-1}_{cat})	Dispersion[e] (%)	Ru particle size (nm)		Ru loading[a] (mmol g^{-1}_{cat})	Ru particle size (nm)		Coke[i] (g_c g_{Ru}^{-1})
						Dispersion[f]	XRD[g] TEM[h]		XRD[g]	TEM[h]	
Ru/γ-Al_2O_3	0.20	124	0.26	11.9	9.2	9.8	14.7 13.6	0.20	22.0	19.6	0.6
Ru/$MgAl_2O_4$	0.19	108	0.28	14.9	10.6	8.5	10.6 8.2	0.21	17.2	20.8	1.4
Ru/Mg_3(Al)O	0.21	128	0.23	17.5	15.2	5.9	– –	0.21	–	–	1.9
Ru/MgO	0.14	24	0.31	14.7	10.5	8.6	– 1.9	0.14	–	3.0	1.3

[a] Measured by ICP.
[b] After calcination at 773 K.
[c] H_2 consumption in H_2-TPR from ambient temperature to 873 K.
[d] Measured by CO chemisorption at room temperature.
[e] Calculated by the equation: dispersion (%) = CO adsorption/(H_2 consumption/2) × 100%, assuming CO/Ru = 1.
[f] Calculated using the equation: particle size = 0.9/dispersion [29].
[g] Calculated by the Scherrer's equation based on the Ru(101) reflection at 2θ = 51.6° by peak fitting.
[h] Measured by TEM.
[i] Measured by TG.

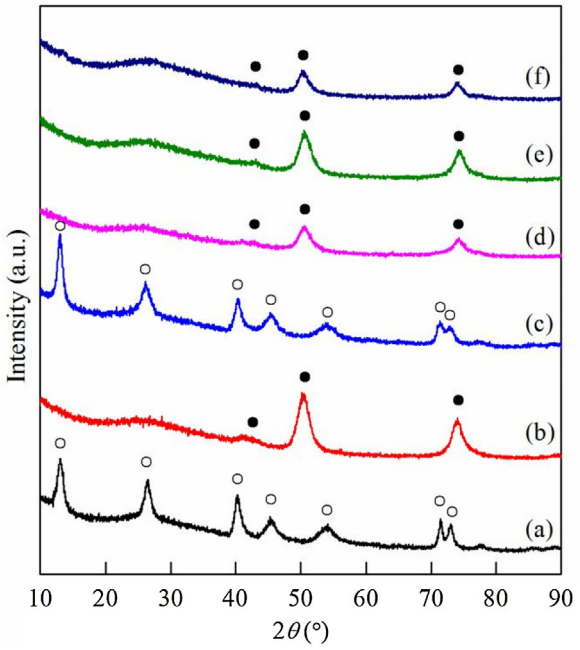

Fig. 1. XRD patterns of the Ru/Mg_3(Al)O catalyst: (a) as-synthesized Mg_3Al LDH, (b) after calcination of LDH at 1073 K, followed by (c) impregnation with $RuCl_3$ aqueous solution, (d) calcination at 773 K, (e) after reduction at 873 K, and (f) after 30 h of reaction at 1023 K. Crystalline phases: (○) Mg_3Al LDH, (●) Mg_3(Al)O.

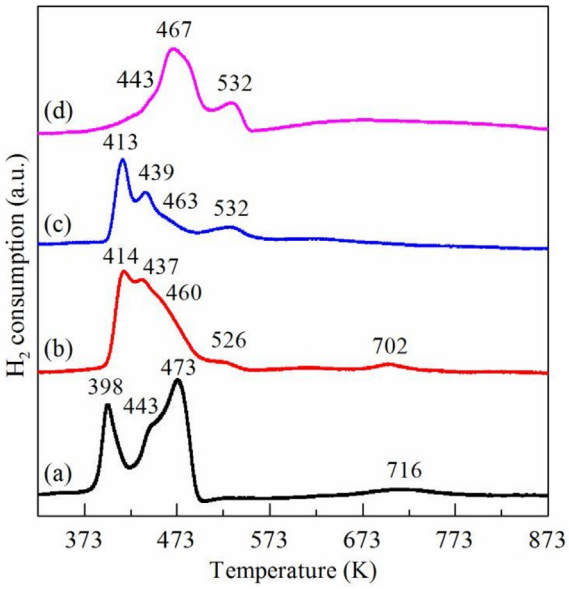

Fig. 2. H_2-TPR profiles of the calcined samples: (a) Ru/γ-Al_2O_3, (b) Ru/$MgAl_2O_4$, (c) Ru/Mg_3(Al)O, and (d) Ru/MgO. Conditions: 10% H_2/Ar, ambient temperature to 873 K, 10 K min^{-1}, sample weight 100 mg.

trating that the 773 K calcination treatment removed a large part of Cl from the as-prepared catalysts. The chemical compositions of the reduced catalysts were also analyzed by SEM-EDX (Supplementary material, Fig. S2 and Table S2), which were basically similar to those of calcined samples.

Fig. 1 shows the XRD patterns of the Ru/Mg_3(Al)O catalyst during the preparation. The XRD pattern of the as-synthesized precursor is characteristic of LDHs, e.g., hydrotalcite $[Mg_6Al_2(OH)_{16}]CO_3{\cdot}4H_2O$ (JCPDS 22-0700). The diffraction peaks at $2\theta = 13.1^\circ$, 26.4°, 40.3°, 45.4°, 54.0°, 71.4°, and 73.0° could be indexed to (003), (006), (012), (015), (018), (110), and (113) reflections, respectively. Upon calcination at 1073 K, the structure of LDH was collapsed and converted to Mg_3(Al)O mixed oxide, which could be attributed to the incorporation of Al^{3+} into the MgO lattice to form a solid solution [31]. When the Mg_3(Al)O mixed oxide was impregnated with $RuCl_3$ aqueous solution, the diffraction peaks of LDH appeared again and the LDH was completely reconstituted by the "memory effect". It is noted that the diffraction peaks of the reconstituted LDH were essentially identical to those of as-synthesized LDH. The memory effect is an interesting property of the LDHs-derived mixed metal oxides, which allows the reconstitution of the original LDH structure when the mixed metal oxide is contacted with aqueous solutions containing various ions [19]. Takehira et al. [21] reported that when Mg-Al mixed oxide was dipped in an aqueous solution of Ni^{2+} nitrate, reconstitution of Mg-Al LDH took place and Ni^{2+} replaced a part of the Mg^{2+} sites to form Mg(Ni)-Al LDH in the surface layer of the Mg-Al mixed oxide. Although the ionic radius of Ru^{3+} (0.068 nm) is similar to those of Ni^{2+} (0.069 nm) and Mg^{2+} (0.072 nm) [32], the study of density functional theory on the octahedral hexahydrated metal cations suggests that Ru^{3+} is less stable for the construction of LDHs due to the structural distortion [33]. Therefore, we consider that the Ru^{3+} precursor was mainly located at the surface of the reconstituted LDH rather than incorporated in the brucite-like layer. It is worth noting that upon calcination no diffraction peaks associated with Ru-containing phase such as RuO_2 could be found, indicating that the Ru oxidic species were highly dispersed. Moreover, no diffraction peaks due to Ru metal were discernable after reduction, indicating that the resulted Ru metal was highly dispersed and the particle size was too small (<3 nm) to detect by XRD. The XRD patterns of the Ru/γ-Al_2O_3, Ru/$MgAl_2O_4$, and Ru/MgO catalysts are presented in Fig. S3 (Supplementary material). In these cases, the diffraction peaks of RuO_2 ($2\theta = 32.6^\circ$, 40.9° and 53.3° JCPDS 40-1290) were detected after impregnation of the support with $RuCl_3$ aqueous solution followed by calcination, and the diffraction peaks of Ru metal ($2\theta = 44.9^\circ$ and 51.6° JCPDS 03-065-7646) were clearly observed after reduction, indicating the formation of larger Ru metal particles, particularly for Ru/γ-Al_2O_3 and Ru/$MgAl_2O_4$. We tried to calculate the size of Ru metal particles by using the Scherrer's equation, but it was difficult to calculate the value properly due to the presence of small Ru metal particles out of the detection limit of XRD (vide infra). For reference, the size of Ru metal particles on Ru/γ-Al_2O_3 and Ru/$MgAl_2O_4$ estimated by the Scherrer's equation based on the diffraction peak at $2\theta = 51.6^\circ$ is listed in Table 1, whereas the size of Ru metal particles on Ru/MgO could not be calculated due to the weak intensity. It is evident from the XRD result that the Ru dispersion was much higher on Ru/Mg_3(Al)O than on Ru/MgO, Ru/$MgAl_2O_4$, and Ru/γ-Al_2O_3.

Fig. 2 shows the H_2-TPR profiles of the calcined samples. All samples displayed several reduction peaks, indicating the presence of different kinds of Ru oxidic species. According to the literatures [34,35], the low-temperature peak centered at 398–414 K might be assigned to the reduction of well-dispersed RuO_x species, and the media-temperature peak centered at 460–473 K might be attributed to the reduction of bulk RuO_2 species, while the high-temperature peaks above 500 K might be ascribed to the reduction of the oxidized Ru species that had strong interaction with the support. A small shoulder peak centered at 437–443 K was also observed, which was probably due to the reduction of undecomposed $RuCl_3$ [36]. Judging from the peak intensity, we considered that Ru/Mg_3(Al)O mainly contained well-dispersed RuO_x, and Ru/MgO mainly contained bulk RuO_2, whereas both well-dispersed RuO_x and bulk RuO_2 co-existed on Ru/γ-Al_2O_3 and Ru/$MgAl_2O_4$. Based on the H_2-TPR profiles, the amount of H_2 consumption was calculated. As shown in Table 1, the amounts of H_2 consumption on Ru/γ-Al_2O_3, Ru/$MgAl_2O_4$, and Ru/Mg_3(Al)O were lower than the stoichiometric values required for the reduction of RuO_2 to metallic Ru, probably due to the presence of irreducible

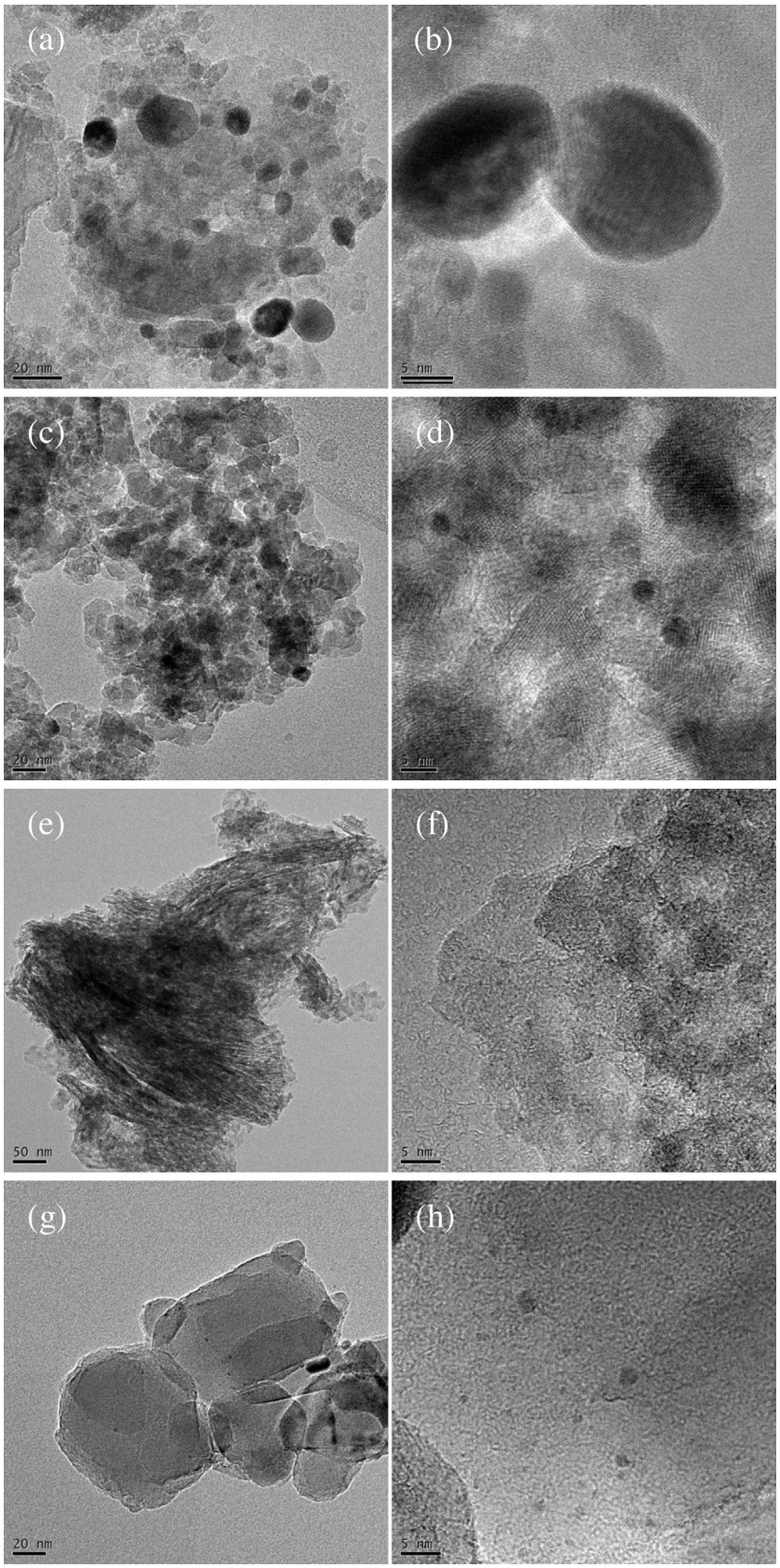

Fig. 3. TEM images of the reduced Ru catalysts: (a, b) Ru/γ-Al_2O_3, (c, d) Ru/$MgAl_2O_4$, (e, f) Ru/Mg_3(Al)O, and (g, h) Ru/MgO.

Ru species. On the other hand, the amount of H_2 consumption on Ru/MgO was slightly higher than that required for the complete reduction of RuO_2, which was probably due to the presence of some high-valence Ru species (e.g. RuO_3 and/or RuO_4 [16]).

Fig. 3 shows representative TEM images of the reduced Ru catalysts. The size-distribution of Ru metal particles is given in Fig. S4 (Supplementary material) and the average particle size estimated by $\Sigma n_i d_i^3/\Sigma n_i d_i^2$ are listed in Table 1. On Ru/γ-Al_2O_3 and Ru/$MgAl_2O_4$, a wide size-distribution of Ru metal particles in the range of 4–22 nm and 2–12 nm was observed, respectively. On the other hand, the Ru metal particles were well dispersed on MgO in the range of 1–3 nm, consistent with previous studies that Ru metal particles tend to be homogeneously distributed on MgO [37–39]. Interestingly, no Ru metal particles were visible on the Ru/Mg_3(Al)O catalyst. This observation combined with the XRD result (Fig. 1e) strongly indicated that the Ru metal was very highly dispersed on the Mg_3(Al)O mixed oxide, probably existing in very small Ru metal nanoparticles and/or clusters. Apparently, the dispersion of Ru metal was Ru/Mg_3(Al)O > Ru/MgO > Ru/$MgAl_2O_4$ > Ru/γ-Al_2O_3, in good agreement with the XRD result.

CO chemisorption was conducted to characterize the accessible surface Ru^0 atoms. The amount of CO adsorption is listed in Table 1. Using a CO/Ru = 1 stoichiometry [40], the number of surface Ru^0 atoms could be calculated, from which the Ru dispersion and particle size could be derived. The amount of CO adsorption was the largest on Ru/Mg_3(Al)O, followed by Ru/$MgAl_2O_4$ and Ru/MgO, while Ru/γ-Al_2O_3 had the smallest CO adsorption. Correspondingly, the Ru dispersion calculated from CO adsorption followed the same tendency. For Ru/γ-Al_2O_3 and Ru/$MgAl_2O_4$, the particle size of Ru metal calculated from the dispersion was comparable or slightly smaller than those determined from XRD and TEM. This might be attributed to the presence of small Ru metal particles that were not counted by XRD and TEM. On the other hand, for Ru/Mg_3(Al)O and Ru/MgO, the Ru particle size calculated from the dispersion was significantly larger than those expected by XRD and TEM. Iwamoto et al. [38] and Xu et al. [39] have reported similar result on Ru/MgO prepared by sol-gel method and by using ethylene glycol as solvent and reductant. One possible explanation is that the small Ru metal particles were partially embedded into the support, leaving only a limited amount of accessible surface Ru^0 atoms.

In order to get more information on the state of surface Ru species, FTIR of CO adsorption was performed. Fig. 4 shows the obtained FTIR spectra of adsorbed CO on the reduced Ru catalysts. All catalysts displayed three CO bands, i.e., 2125–2133 cm^{-1}, 2069–2081 cm^{-1}, and 2000–2025 cm^{-1}, similar to those reported in the literatures [29,41,42]. In general, the CO bands originated from CO adsorption on supported Ru catalysts are divided into three groups: high frequency 1 (HF_1) at 2156–2133 cm^{-1}, high frequency 2 (HF_2) at 2100–2060 cm^{-1}, and low frequency (LF) at 2060–1970 cm^{-1}. The LF band was assigned to the linearly adsorbed CO on metallic Ru (Ru^0-CO), and the HF_1 and HF_2 bands were attributed to CO adsorption on partially oxidized Ru sites ($Ru^{\delta+}$-CO), which were produced by the oxidative disruption of very small Ru cluster with the participation of hydroxyl groups of the support [41,42]. It should be noted that the wavenumber and intensity of the CO bands on the Ru catalysts changed with the support used. Comparing the peak intensity, it can be seen that the HF/LF intensity ratio increased in the order: Ru/γ-Al_2O_3 (0.62) < Ru/$MgAl_2O_4$ (0.67) < Ru/Mg_3(Al)O (0.86) < Ru/MgO (0.98). The relatively higher HF/LF intensity ratio on Ru/Mg_3(Al)O and Ru/MgO indicated that Ru clusters and/or very small Ru particles were more dominant on these two catalysts, in agreement with the TEM measurement. Meanwhile, it can be seen that the linear CO band was shifted to lower wavenumber in the sequence of Ru/γ-Al_2O_3 > Ru/$MgAl_2O_4$ > Ru/MgO > Ru/Mg_3(Al)O. The low-wavenumber shift might be explained by the particle size effect.

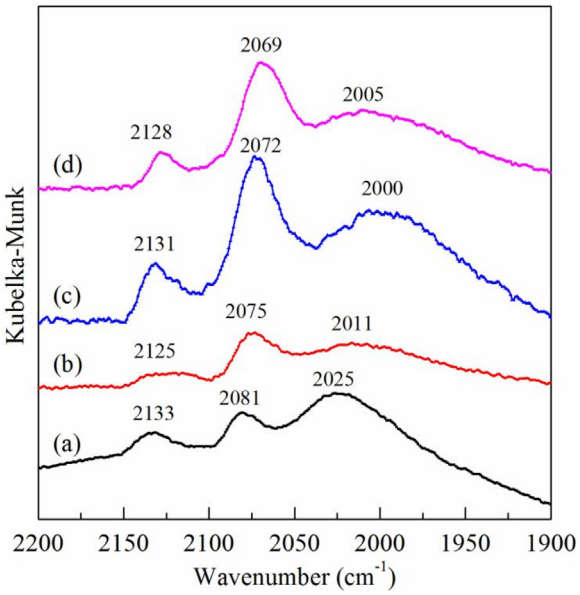

Fig. 4. FTIR spectra of adsorbed CO on the reduced Ru catalysts: (a) Ru/γ-Al_2O_3, (b) Ru/$MgAl_2O_4$, (c) Ru/Mg_3(Al)O, and (d) Ru/MgO.

Generally, with the decrease of metal particle size, the fraction of face atoms would decrease and those of corner atoms and edge atoms would increase. Since the corner atoms and edge atoms are more coordinately unsaturated, this might cause a higher degree of back-donation of electrons into the antibonding π^* orbital of CO, weakening the strength of C—O bond and causing a low-wavenumber shift [43,44].

XPS was further employed to study the chemical state of Ru species. Fig. 5 shows the Ru 3d spectra of the reduced Ru catalysts. The C1s peak at 284.6 eV, which was due to carbonaceous contamination, has been taken as the reference for the binding energy values. The C 1 s spectra also displayed two peaks at 286.8 and 289.0 eV that could be attributed to carbonaceous species associated with oxygen and/or hydrogen [16]. For all catalysts, two Ru 3d5/2 peaks at 279.6–280.7 and 280.8–282.4 eV could be observed. The former was assigned to metallic Ru^0, whereas the latter might be attributed to partially oxidized Ru species [15,16,37,45]. It is worth noting that the binding energy of Ru^0 was much higher on Ru/Mg_3(Al)O (280.7 eV) than on Ru/γ-Al_2O_3 (279.6 eV), Ru/$MgAl_2O_4$ (279.8 eV), and Ru/MgO (280.0 eV), which was also higher than that reported for bulk Ru (279.6–280.2 eV) [45], indicating a stronger interaction between the Ru metal particles and the Mg_3(Al)O mixed oxide. Such high binding energy might also be related to the finely dispersed Ru metal particles [46]. Mason et al. [47] have reported that small metal particles (Pd, Pt, Au) on carbonaceous support processed higher binding energies than bulk metals. The typical binding energy increased by 1 eV and only small (no more than 10 atoms) clusters of metal were affected this way. Ryndin et al. [48] have also reported that the binding energy of Pd^0 on Pd/C increased with increasing the Pd dispersion. Thus, the XPS result was generally in agreement with the TEM measurement, confirming the formation of very highly dispersed Ru metal on Ru/Mg_3(Al)O.

It has been reported that the basic property of support plays an important role for the adsorption and activation of CO_2 [49,50]. According to the literature [51], the reactive adsorption of CO_2 as an acidic molecule on basic sites may lead to the formation of several forms of carbonate species: monodentate, bidentate, and bicarbonate anions. Monodentate carbonate involves low-coordination oxygen anions and accounts for strong basic sites. Bidentate carbonates form on acid-base pairs, such as Mg^{2+}-O^{2-} or Al^{3+}-O^{2-},

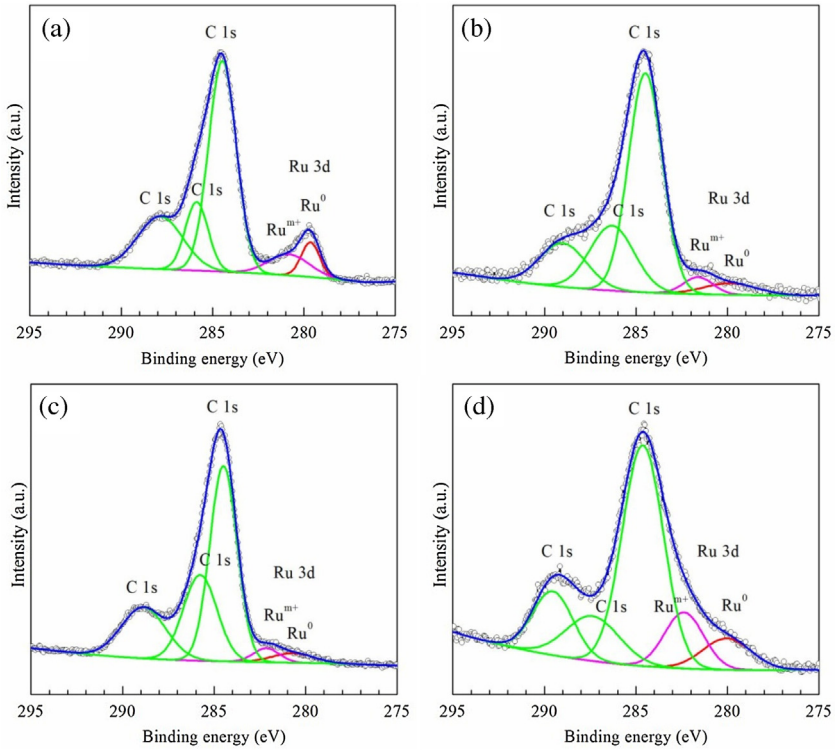

Fig. 5. Ru 3d5/2 XPS of the reduced Ru catalysts: (a) Ru/γ-Al_2O_3, (b) Ru/$MgAl_2O_4$, (c) Ru/Mg_3(Al)O, and (d) Ru/MgO.

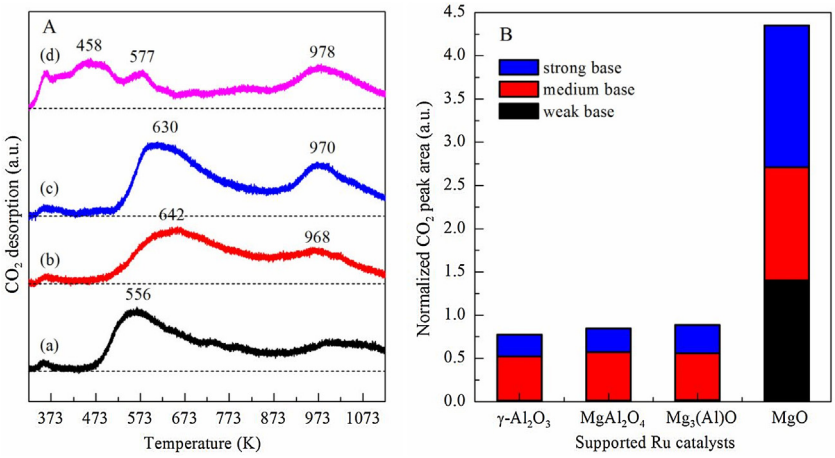

Fig. 6. (A) CO_2-TPD profiles of the reduced Ru catalysts: (a) Ru/γ-Al_2O_3, (b) Ru/$MgAl_2O_4$, (c) Ru/Mg_3(Al)O, and (d) Ru/MgO. (B) CO_2 peak areas normalized by the BET surface area.

corresponding to intermediate strength base sites. The formation of bicarbonate anions requires surface hydroxyl groups that can be considered as weak base sites (e.g. Mg-OH) or acid sites (e.g. Al-OH). CO_2-TPD profiles obtained on the reduced Ru catalysts are shown in Fig. 6. On Ru/γ-Al_2O_3, a strong CO_2 desorption peak was observed at 556 K together with a small peak above 873 K; these peaks could be associated with the decomposition of carbonate-like species, corresponding to intermediate strength and strong basic sites, respectively. In the cases of Ru/$MgAl_2O_4$ and Ru/Mg_3(Al)O, the CO_2 desorption peaks were observed at about 642 K and 968 K. Compared to that of Ru/γ-Al_2O_3, the medium-temperature peak was remarkably shifted to higher temperature, suggesting that the strength of intermediate base was higher on Ru/$MgAl_2O_4$ and Ru/Mg_3(Al)O than on Ru/γ-Al_2O_3. This might be explained as due to the presence of Mg^{2+}-O^{2-} pairs. For Ru/MgO, the CO_2 desorption peaks were mainly observed at 978 K, 577 K and 458 K; the low-temperature peak might be attributed to desorption of CO_2 on weak basic sites. From the CO_2-TPD profiles, the areas of CO_2 desorption peaks were calculated (Supplementary material, Fig. S5) and the normalized values with respect to BET surface area are shown in Fig. 6B. The total amount of basic sites was similar for all catalysts. Nevertheless, considering the BET surface area, the amount of basic sites per square meter (base intensity) was remarkably higher on Ru/MgO, while the other three catalysts showed low and similar values. For example, the intensity of strong base on Ru/MgO was approximately 5.8 times those on the other catalysts. This result revealed the strong basic characteristic of MgO. The base intensity was much weak on Mg_3(Al)O as compared to MgO, probably due to the surface modification of MgO with Al [52].

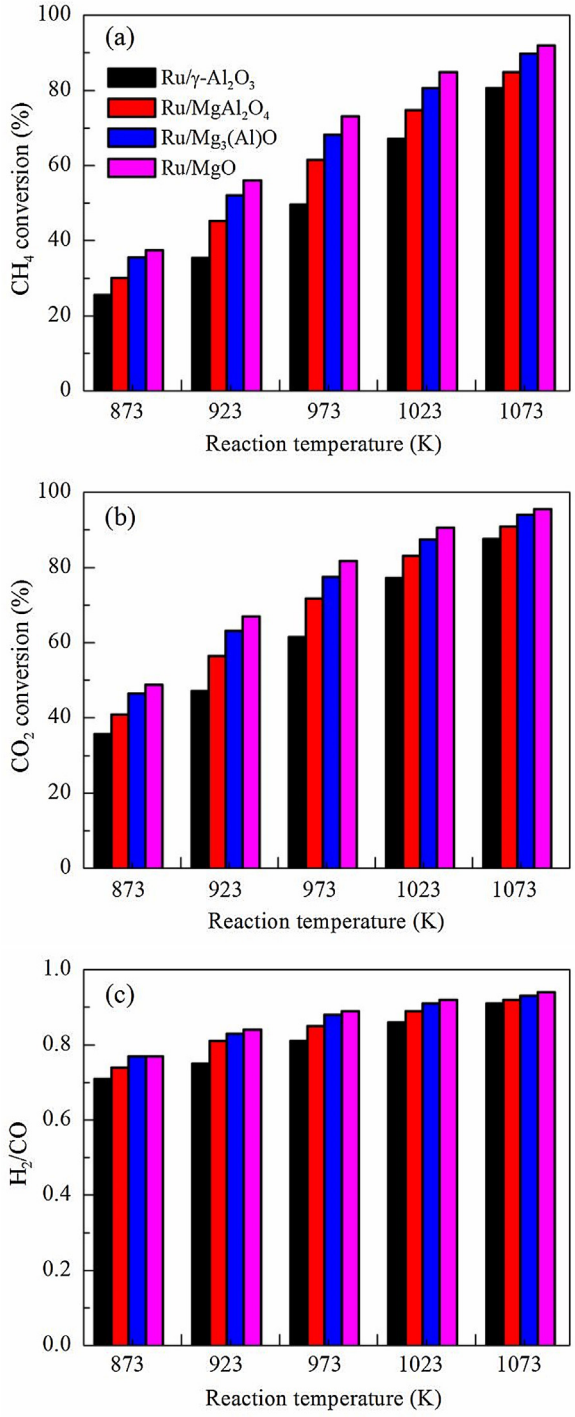

Fig. 7. Catalytic activity of Ru catalysts for the CH_4-CO_2 reforming at different reaction temperatures: (a) CH_4 conversion, (b) CO_2 conversion, and (c) H_2/CO ratio. Reaction conditions: CH_4:CO_2:N_2 = 1:1:2, WHSV = 60,000 mL g^{-1} h^{-1}; reaction time, 1 h at each temperature; catalyst, 50 mg, pre-reduced with H_2 at 873 K for 0.5 h.

3.2. Catalytic activity in CH_4-CO_2 reforming

Fig. 7 compares the CH_4-CO_2 reforming activities of the Ru catalysts at different reaction temperatures. The activity was tested at elevated temperatures from 873 K to 1073 K with CH_4: CO_2: N_2 = 1:1:2 and WHSV = 60,000 mL g^{-1} h^{-1} after the catalyst was reduced with H_2 at 873 K for 0.5 h. At each temperature, the activity was evaluated for 1 h, and the CH_4 conversion, CO_2 conversion, and H_2/CO ratio were calculated based on the average value. For all catalysts, both the CH_4 and CO_2 conversions increased with increasing the reaction temperature, which is favored by the fact that CH_4-CO_2 reforming is a highly endothermic reaction and higher temperature is favorable for the equilibrium shift toward syngas production. In addition, the CO_2 conversion was always higher than that of CH_4, and the H_2/CO ratio was less than 1 especially at low temperatures, which was due to the reverse water-gas shift reaction (RWGS: $CO_2 + H_2 \rightarrow CO + H_2O$ ΔH_{298K} = 41 kJ mol^{-1}). Under the present reaction conditions, the conversions of CH_4 and CO_2 on all catalysts were below the equilibrium values calculated from the thermodynamic data of CH_4-CO_2 reforming and RWGS. Judging from the conversions of CH_4 and CO_2, the order of catalytic activity was Ru/MgO > $Ru/Mg_3(Al)O$ > $Ru/MgAl_2O_4$ > Ru/γ-Al_2O_3. Based on the CH_4 conversion at 873 K and the amount of CO adsorption, the CH_4 turnover frequency (TOF) was calculated, which was 4.0, 3.8, 3.8, and 4.7 s^{-1} for Ru/γ-Al_2O_3, $Ru/MgAl_2O_4$, $Ru/Mg_3(Al)O$, and Ru/MgO, respectively. The TOF of Ru/MgO was slightly higher than those of Ru/γ-Al_2O_3, $Ru/MgAl_2O_4$, and $Ru/Mg_3(Al)O$. This might be related to the high intensity of strong base on Ru/MgO. It has been suggested that the strong basic sites would favor the adsorption and dissociation of CO_2, providing more "active oxygen" species on the catalyst surface and enhancing the gasification of carbonaceous species [10,50]. The TOF of $Ru/Mg(Al)O$ was slightly low, but its catalytic activity was comparable with that of Ru/MgO, which could be attributed to the larger number of surface Ru^{00} atoms. One point should be noted is that the TOF difference of the catalysts was much small as compared to the great discrepancy in the Ru particle size, suggesting that the reaction rate was not significantly affected by Ru particle size. The structure sensitivity of CH_4-CO_2 reforming has been discussed by Mark and Maier [53] over Rh and Ir catalysts supported on different oxides including Al_2O_3, SiO_2, ZrO_2, TiO_2, and SiO_2-based mixed oxides. They found that the TOF was independent on the nature of the support and the metal dispersion and that the activity depended only on the number of the accessible metal surface area, indicative of structure insensitivity of the reaction. This is generally in agreement with our result.

3.3. Catalytic stability in CH_4-CO_2 reforming

To measure the catalyst stability, the CH_4-CO_2 reforming was carried out at 1023 K and W/F = 60,000 mL g^{-1} h^{-1}, at which the conversions of CH_4 and CO_2 were lower than the equilibrium values calculated from the thermodynamic data of CH_4-CO_2 reforming and RWGS. Fig. 9 shows the changes of catalytic activity with time on stream over the Ru catalysts. Unfortunately, a significant deactivation was observed on Ru/γ-Al_2O_3, $Ru/MgAl_2O_4$, and Ru/MgO catalysts, all of which showed a similar linear decrease in the CH_4 and CO_2 conversions and H_2/CO ratio. After 30 h of reaction, the CH_4 conversion decreased from initial 68%, 75%, and 83% to 55%, 61%, and 70%, and the CO_2 conversion decreased from initial 77%, 83%, and 89% to 64%, 72%, and 80% for Ru/γ-Al_2O_3, $Ru/MgAl_2O_4$, and Ru/MgO, respectively. The deactivation rate was calculated to be approximately 0.43% h^{-1} based on the CH_4 conversion. It is worth noting that the $Ru/Mg_3(Al)O$ catalyst showed very stable activity during 30 h of reaction, the conversions of CH_4 and CO_2 being almost the same with the initial levels of 84% and 90%, respectively. The catalytic stability of $Ru/Mg_3(Al)O$ was superior than those of Ru/γ-Al_2O_3, $Ru/MgAl_2O_4$, and Ru/MgO. To verify the superior stability of $Ru/Mg_3(Al)O$, a 300 h of long-term test was further conducted. As shown in Fig. 9, the $Ru/Mg_3(Al)O$ catalyst exhibited excellent stability during the whole time on stream investigated, demonstrating a promising catalyst for the CH_4-CO_2 reforming.

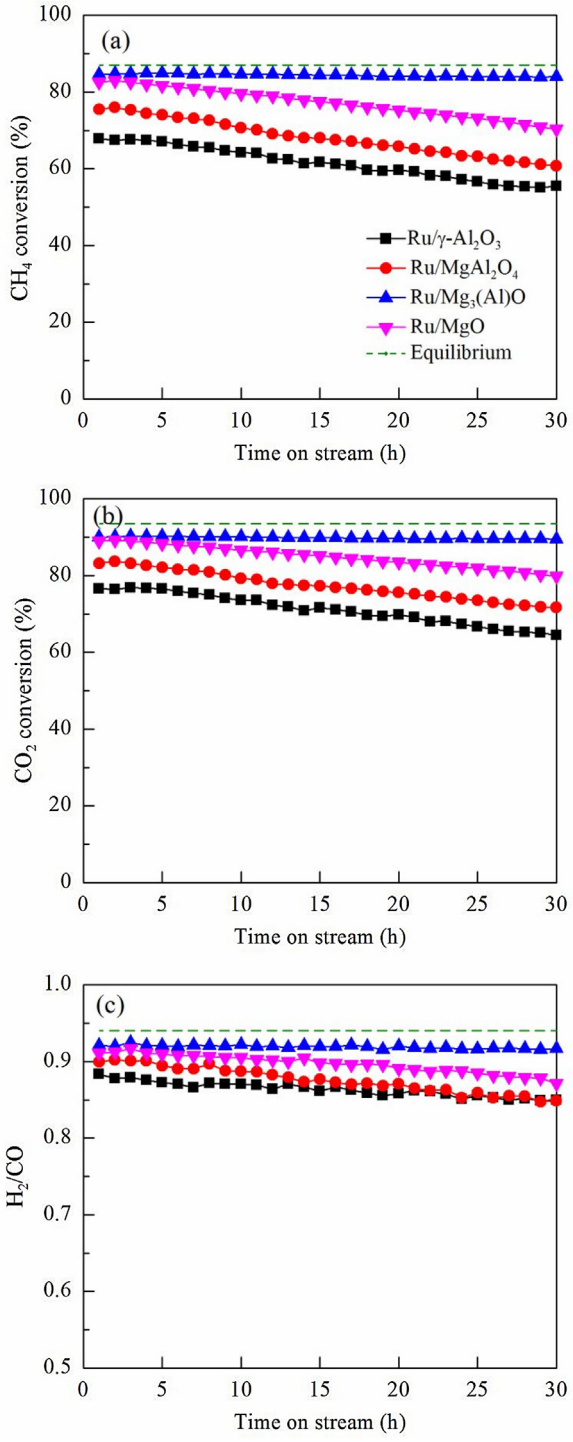

Fig. 8. Catalytic stability of the Ru catalysts for the CH_4-CO_2 reforming: (a) CH_4 conversion, (b) CO_2 conversion, (c) H_2/CO ratio. Reaction conditions: CH_4:CO_2:N_2 = 1:1:2, WHSV = 60,000 mL g^{-1} h^{-1}, T = 1023 K; catalyst 50 mg, pre-reduced with H_2 at 873 K for 0.5 h.

3.4. Characterization of the spent catalysts

To understand the causes for the different catalytic stabilities of the prepared Ru catalysts, the spent catalysts after 30 h of reaction were characterized by various techniques. According to the literatures [8,54,55], the deactivation of Ru catalysts in the CH_4-CO_2 reforming may be caused by coke deposition, sintering of Ru metal particles, and oxidation of metallic Ru. In addition, the loss of Ru species was also reported in the literature [30]. Therefore, a combination of ICP, Raman, TG, XRD, and TEM were used to analysis the Ru loading, coke deposition, Ru particle size, and Ru oxidic species.

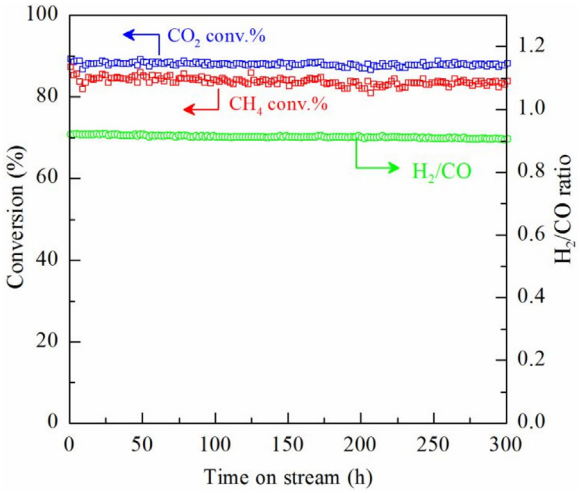

Fig. 9. Long-term stability of the Ru/Mg_3(Al)O catalyst in the CH_4-CO_2 reforming. Reaction conditions are the same with those in Fig. 8.

As shown in Table 1, the Ru loading on the spent catalyst was similar to the initial value within the experimental error, indicating that no or little Ru species were lost during the reaction. Thus, the loss of Ru species should not be responsible for the catalyst deactivation. It is well known that species such as Na^+ and Cl^- ions remaining in the catalyst can poison the active sites. The SEM-EDX analysis on the calcined and reduced catalysts indicated that the contents of residual Na^+ and Cl^- ions in the catalyst were low and similar for each catalyst. Although the influence of Na^+ and Cl^- ions on the catalytic stabilities of Ru/γ-Al_2O_3, Ru/$MgAl_2O_4$, and Ru/MgO cannot be excluded, it is reasonable to consider that Na^+ and Cl^- ions had little effect on Ru/Mg_3(Al)O considering its good catalytic stability.

Raman spectroscopy was employed to probe the structure of coke deposited on the spent catalysts and the obtained Raman spectra are presented in Fig. 10A. No signals at 1200–1800 cm^{-1} due to carbonaceous species were detected on Ru/γ-Al_2O_3, indicating that little graphitic carbon was formed. On the other hand, Ru/$MgAl_2O_4$, Ru/Mg_3(Al)O, and Ru/MgO displayed two bands at about 1325 cm^{-1} and 1591 cm^{-1}, corresponding to the defect (D band) and graphite (G band), respectively [56]. The G band is characteristic of graphitic carbon, which arises from the in-plane carbon–carbon stretching vibration of pairs of sp^2 carbons, whereas the D band is induced by the disorders or defects due to structural imperfections, and it exists extensively in polycrystalline and defective graphite as well as other carbonaceous materials. The integral intensity ratio of I(D)/I(G) was determined to Ru/Mg_3(Al)O (0.71) < Ru/$MgAl_2O_4$ (1.15) < Ru/MgO (1.26), suggesting higher crystallinity of carbon on the Ru/Mg_3(Al)O catalyst. The amount of coke deposited on the spent catalyst was measured by TG analysis. The TG profiles and the 1st derivative of TG curve are shown in Fig. 10B. All catalysts showed one weight loss below 473 K, attributable to physically adsorbed water. Additional weight loss at 473–773 K was observed, which could be assigned to the combustion of highly reactive monoatomic carbon [57]. No significant weight loss above 773 K was found, indicating that little filamentous carbon was formed [58]. The amount of carbon was calculated based on the weight loss at 473–873 K and was normalized with respect to the Ru loading. As listed in Table 1, the amount of carbon was 0.6–1.9 g_c g_{Ru}^{-1}, which was <0.01% of the total fed carbon during 30 h of reaction, confirming the good coke-resistance of Ru. It is noted that the amount of

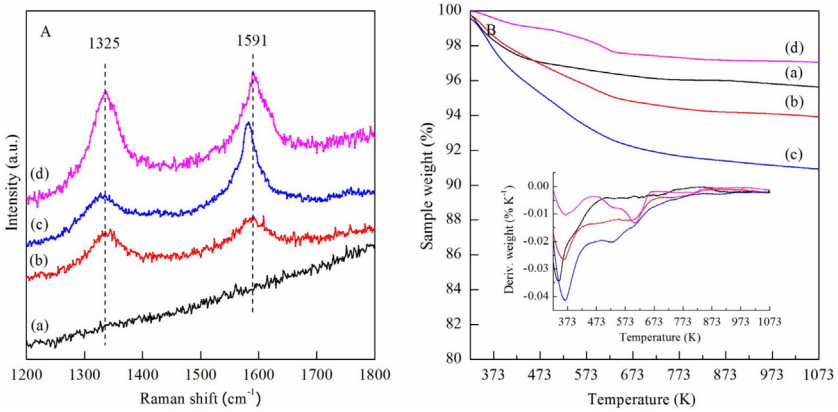

Fig. 10. (A) Raman spectra and (B) TG analysis of deposited coke on the spent Ru catalysts (Fig. 8): (a) Ru/γ-Al_2O_3, (b) Ru/$MgAl_2O_4$, (c) Ru/Mg_3(Al)O, and (d) Ru/MgO.

carbon was slightly higher on Ru/Mg_3(Al)O than on Ru/γ-Al_2O_3, Ru/$MgAl_2O_4$, and Ru/MgO. This was correlated with the high activity of Ru/Mg_3(Al)O. Monoatomic carbon is highly reactive and is not responsible for the catalyst deactivation. Therefore, it is reasonable to consider that coke deposition was not the main cause for the catalyst deactivation.

The XRD pattern of the Ru/Mg_3(Al)O spent catalyst is presented in Fig. 1(f) and those of the Ru/γ-Al_2O_3, Ru/$MgAl_2O_4$, and Ru/MgO spent catalysts are shown in Fig. S3(f), respectively. No significant changes in the XRD patterns between the reduced catalyst and the spent catalyst were observed for all catalysts, suggesting that the crystalline structure of supports was thermally stable. This is expected for Ru/γ-Al_2O_3 and Ru/$MgAl_2O_4$ since the supports was obtained by calcination of the precursors at 1073 K, which was higher than the reaction temperature. In the cases of Ru/MgO and Ru/Mg_3(Al)O, MgO and Mg_3(Al)O were reconstituted to $Mg(OH)_2$ and Mg_3Al LDH during the impregnation procedure and then calcined at low temperature of 773 K. Although the reaction temperature was higher than the thermal treatment temperature, the crystalline size of MgO remained almost the same (27.6 nm and 27.0 nm before and after reaction). This could be attributed to the well crystallinity of MgO. In the case of Ru/Mg_3(Al)O, only a slight increase in the crystalline size of Mg_3(Al)O was observed (5.2 nm and 7.0 nm before and after reaction). This is generally in agreement with that the LDHs-derived Mg(Al)O mixed oxides are well-dispersed and thermally stable. These results indicated that all the supports were thermally stable under the reaction conditions. In the XRD patterns, no peaks associated with graphite carbon were presented, indicating that graphite carbon was little formed, in agreement with the TG result. In addition, no peaks corresponding to RuO_2 phase were detectable, which was consistent with the Raman result that no signals at 600–700 cm^{-1} related to RuO_x species [15] were observed (Supplementary material, Fig. S6). The oxidation of metallic Ru with CO_2 has been reported [8,15,54] and in some cases it was related to the catalyst deactivation [8,54]. The absence of RuO_2 and/or RuO_x on the spent catalysts suggests that the oxidation of metallic Ru was limited under the present reaction conditions and should not be responsible for the catalyst deactivation. The average particle size of Ru metal was calculated by the Scherrer's equation based on the (101) diffraction peak of Ru metal at $2\theta = 51.6^\circ$, as shown in Table 1. For Ru/γ-Al_2O_3 and Ru/$MgAl_2O_4$, the particle sizes became larger than those freshly reduced ones, indicating the sintering of Ru metal particles. Nevertheless, it was difficult to calculate the particle size of Ru/MgO properly, and no diffraction peaks due to Ru metal were detectable on Ru/Mg_3(Al)O, similar to the case of the freshly reduced catalyst.

The particle size of Ru metal was further investigated by TEM. Fig. 11 shows typical TEM images of the spent Ru catalysts. The size distribution of Ru metal particles is given in Fig. S7 (Supplementary material) and the average particle size calculated by $\Sigma n_i d_i^3 / \Sigma n_i d_i^2$ is presented in Table 1. As compared to those of freshly reduced catalysts, the average size of Ru metal particles on the Ru/γ-Al_2O_3 and Ru/$MgAl_2O_4$ catalysts was increased. This is in line with the XRD result, confirming the sintering of Ru metal particles. Sintering of Ru metal particles was also observed by TEM on the Ru/MgO catalyst, where the average particle size increased from 1.9 nm to 3.1 nm. It is well known that sintering of metal particles would decrease the number of surface active sites and as a result cause catalyst deactivation. Thus, we attributed the deactivation of Ru/γ-Al_2O_3, Ru/$MgAl_2O_4$, and Ru/MgO mainly to the sintering of Ru metal particles. In the case of Ru/Mg_3(Al)O, the Ru metal was still invisible, in good agreement with the XRD result. Both the TEM and XRD measurements clearly showed that the size of Ru metal particles on the Ru/Mg_3(Al)O spent catalyst was too small to detect, similar to that of the freshly reduced catalyst. We thus considered that the highly dispersed Ru metal on Ru/Mg_3(Al)O was stable during the long-term CH_4-CO_2 reforming.

Our results clearly showed that the Ru metal supported on the Mg_3(Al)O mixed oxide was very highly dispersed and much stable than those supported on MgO, γ-Al_2O_3, and $MgAl_2O_4$, demonstrating the significant effect of Mg_3(Al)O support on the improvement of Ru dispersion and catalytic performance. It is noted that the BET surface area of Ru/Mg_3(Al)O was comparable to those of Ru/γ-Al_2O_3 and Ru/$MgAl_2O_4$, but the Ru dispersion was significantly higher on Ru/Mg_3(Al)O, suggesting that there might exist an strong metal-support interaction between Ru and Mg_3(Al)O. Similar strong metal-support interaction between Ru and MgO on Ru/MgO might also be expected considering its much lower BET surface area and higher Ru dispersion than those of Ru/γ-Al_2O_3 and Ru/$MgAl_2O_4$. It was reported [59] that an epitaxial interaction existed in the RuO_2/MgO system between (110) RuO_2 and (100) MgO layers, and Larichev [45] suggested that such epitaxial interaction would stabilize RuO_2 nanoparticles. Based on these reports and the results described above, the formation of highly dispersed and stable Ru metal on Mg_3(Al)O might be explained as follows. During the impregnation of $RuCl_3$ solution with Mg_3(Al)O, Mg_3(Al)O was reconstituted to Mg_3Al LDH, meanwhile, $RuCl_3$ was partially hydrolyzed to form $Ru(OH)_x$ and attached to the LDH surface. Upon calcination, the $Ru(OH)_x$ species were decomposed to RuO_x and interacted closely with the Mg_3(Al)O mixed oxide. The low crystalline Mg_3(Al)O mixed oxide had rough surface and possessed many surface defects, which might act as anchoring sites for the RuO_x species. Meanwhile, the epitaxial interaction between RuO_x and Mg(Al)O would stabilize the RuO_x species. As a result, well-dispersed RuO_x species could be formed. It could thus be expected that the reduction of these well-dispersed RuO_x species

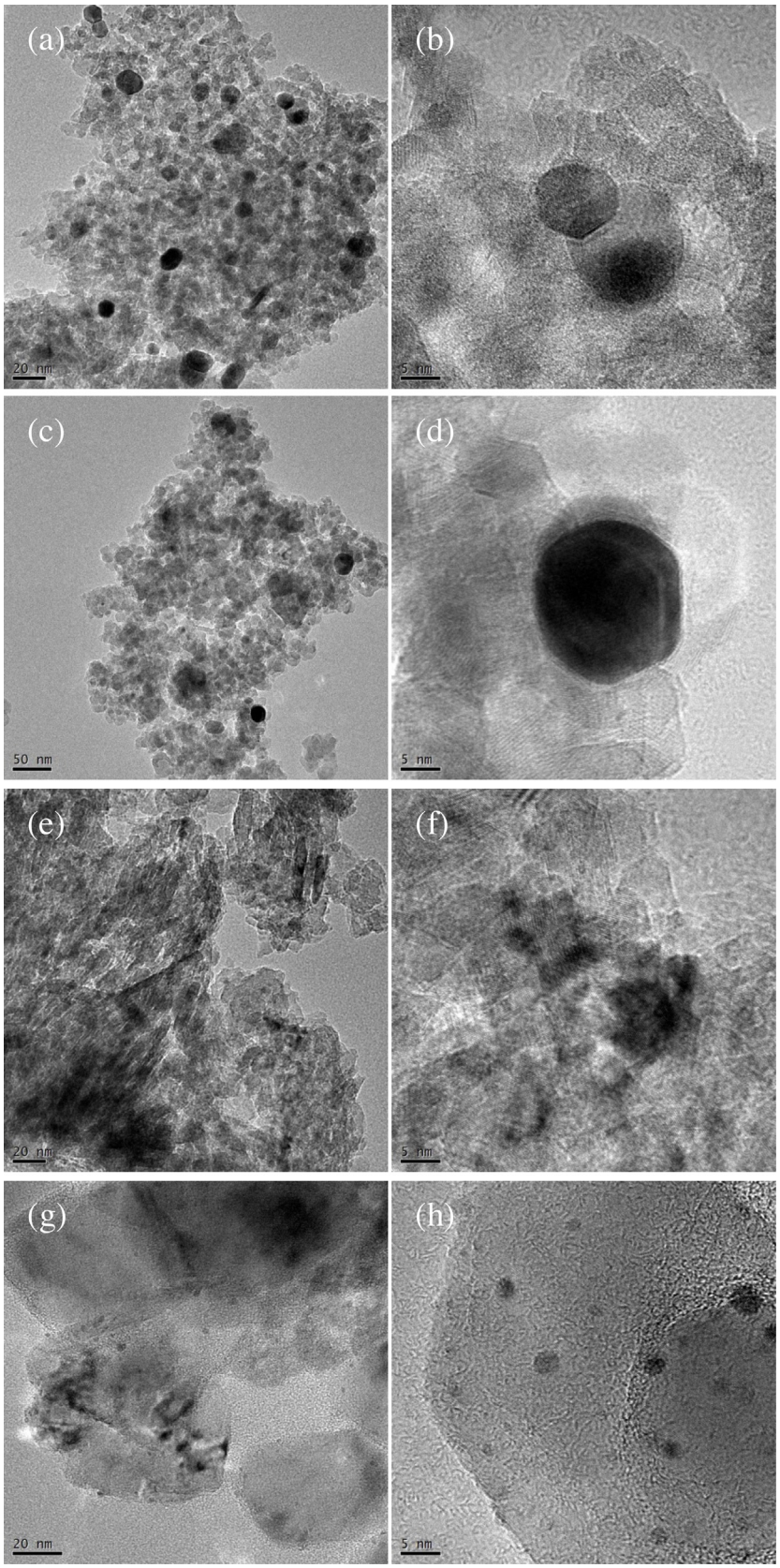

Fig. 11. TEM images of the spent Ru catalysts (Fig. 8): (a, b) Ru/γ-Al_2O_3, (c, d) Ru/$MgAl_2O_4$, (e, f) Ru/Mg_3(Al)O, and (g, h) Ru/MgO.

would give rise to very small Ru nanoparticles and/or clusters. From the CO chemisorption, it could be inferred that the small Ru nanoparticles/clusters were partially embedded into the Mg_3(Al)O support. This might account for their thermal stability in the high-temperature CH_4-CO_2 reforming. In the case of Ru/MgO, similar effects might take place. Nevertheless, owing to the high crys-

tallinity and low surface area, the surface of MgO was expected to be smoother and less defects, which would cause the agglomeration of RuO_x species leading to small-sized RuO_2 and consequently small-sized Ru particles. In the cases of Ru/γ-Al_2O_3 and Ru/$MgAl_2O_4$, the $RuCl_3$ precursor was less hydrolyzed. The unhydrolyzed $RuCl_3$ precursor was weakly adsorbed on the support surface, resulting in large bulk RuO_2 and large Ru particles upon calcination and reduction treatments and consequently leading to poor thermal stability.

4. Conclusion

Ru catalysts supported on Mg and/or Al oxides including γ-Al_2O_3, $MgAl_2O_4$, Mg_3(Al)O, and MgO showed great differences in the Ru metal dispersion and catalytic performance for the CH_4-CO_2 reforming. The Ru metal dispersion was Ru/Mg_3(Al)O > Ru/MgO > Ru/$MgAl_2O_4$ > Ru/γ-Al_2O_3. Particularly, the Ru metal was very highly dispersed on the Mg_3(Al)O mixed oxide, probably existing in very small nanoparticles and/or clusters. The activities of Ru/MgO and Ru/Mg_3(Al)O were higher than those of Ru/$MgAl_2O_4$ and Ru/γ-Al_2O_3, which might be related to the strong base intensity of support and more accessible surface Ru^0 atoms, respectively. When the catalysts were tested at 1023 K for 30 h, a significant deactivation was observed on Ru/γ-Al_2O_4, Ru/$MgAl_2O_4$, and Ru/MgO, while Ru/Mg_3(Al)O showed superior stability. The characterization on the spent catalysts suggests that sintering of Ru metal particles was mainly responsible for the catalyst deactivation. In contrast, the highly dispersed Ru metal on Mg_3(Al)O was stable and no significant sintering of Ru metal was visible. The excellent stability of Ru/Mg_3(Al)O was further confirmed in 300 h long-term test, demonstrating a promising catalyst for the CH_4-CO_2 reforming.

Acknowledgments

This work was financially supported by National Nature Science Foundation of China (No. 21576052), National High Technology Research and Development Program of China (863 Program, No.2015AA03A402, No. 2015AA050502), and Natural Science Foundation of Fujian Province (No.2015J01050).

Appendix A. Supplementary data

Supplementary data associated with this article can be found, in the online version, at http://dx.doi.org/10.1016/j.apcatb.2016.07.050.

References

[1] D.S.A. Simakov, M.M. Wright, S. Ahmed, E.M.A. Mokheimer, Y. Roman-Leshkov, Catal. Sci. Technol. 5 (2015) 1991–2016.
[2] S. Kawi, Y. Kathiraser, J. Ni, U. Oemar, Z. Li, E.T. Saw, ChemSusChem 8 (2015) 3556–3575.
[3] D. Pakhare, J. Spivey, Chem. Soc. Rev. 43 (2014) 7813–7837.
[4] D. Li, Y. Nakagawa, K. Tomishige, Appl. Catal. A: Gen. 408 (2011) 1–24.
[5] F. Solymosi, G. Kutsán, A. Erdöhelyi, Catal. Lett. 11 (1991) 149–156.
[6] J.R. Rostrup-Nielsen, J.H.B. Hansen, J. Catal. 144 (1993) 38–49.
[7] M.C.J. Bradford, M. Albert Vannice, Catal. Today 50 (1999) 87–96.
[8] D.C. Carvalho, H.S.A. de Souza, J.M. Filho, A.C. Oliveira, A. Campos, É.R.C. Milet, F.F. de Sousa, E. Padron-Hernandez, A.C. Oliveira, Appl. Catal. A: Gen. 473 (2014) 132–145.
[9] P. Ferreira-Aparicio, C. Marquez-Alvarez, I. Rodriguez-Ramos, Y. Schuurman, A. Guerrero-Ruiz, C. Mirodatos, J. Catal. 184 (1999) 202–212.
[10] N. Matsui, K. Anzai, N. Akamatsu, K. Nakagawa, N. Ikenaga, T. Suzuki, Appl. Catal. A: Gen. 179 (1999) 247–256.
[11] M.C.J. Bradford, M.A. Vannice, J. Catal. 183 (1999) 69–75.
[12] K. Nagaoka, M. Okamura, K. Aika, Catal. Commun. 2 (2001) 255–260.
[13] A. Derk, G. Moore, S. Sharma, E. McFarland, H. Metiu, Top. Catal. 57 (2014) 118–124.
[14] J. Chen, C. Yao, Y. Zhao, P. Jia, Int. J. Hydrogen Energy 35 (2010) 1630–1642.
[15] B.M. Faroldi, J.F. Múnera, L.M. Cornaglia, Appl. Catal. B: Environ. 150–151 (2014) 126–137.
[16] S. Gaur, D. Pakhare, H. Wu, D.J. Haynes, J.J. Spivey, Energy Fuels 26 (2012) 1989–1998.
[17] U.L. Portugal, C.M.P. Marques, E.C.C. Araujo, E.V. Morales, M.V. Giotto, J.M.C. Bueno, Appl. Catal. A: Gen. 193 (2000) 173–183.
[18] B. Faroldi, S. Irusta, L. Cornaglia, Appl. Catal. A: Gen. 504 (2015) 391–398.
[19] F. Cavani, F. Trifirò, A. Vaccari, Catal. Today 11 (1991) 173–301.
[20] H.A. Prescott, Z. Li, E. Kemnitz, A. Trunschke, J. Deutsch, H. Lieske, A. Auroux, J. Catal. 234 (2005) 119–130.
[21] K. Takehira, T. Kawabata, T. Shishido, K. Murakami, T. Ohi, D. Shoro, M. Honda, K. Takaki, J. Catal. 231 (2005) 92–104.
[22] K. Takehira, T. Shishido, P. Wang, T. Kosaka, K. Takaki, J. Catal. 221 (2004) 43–54.
[23] D. Li, I. Atake, T. Shishido, Y. Oumi, T. Sano, K. Takehira, J. Catal. 250 (2007) 299–312.
[24] D. Li, L. Wang, M. Koike, Y. Nakagawa, K. Tomishige, Appl. Catal. B: Environ. 102 (2011) 528–538.
[25] D. Li, M. Koike, L. Wang, Y. Nakagawa, Y. Xu, K. Tomishige, ChemSusChem 7 (2014) 510–522.
[26] D. Li, M. Lu, K. Aragaki, M. Koike, Y. Nakagawa, K. Tomishige, Appl. Catal. B: Environ. 192 (2016) 171–181.
[27] P. Seetharamulu, V. Siva Kumar, A.H. Padmasri, B. David Raju, K.S. Rama Rao, J. Mol. Catal. A: Chem. 263 (2007) 253–258.
[28] A.I. Tsyganok, M. Inaba, T. Tsunoda, S. Hamakawa, K. Suzuki, T. Hayakawa, Catal. Commun. 4 (2003) 493–498.
[29] B.M. Faroldi, E.A. Lombardo, L.M. Cornaglia, Appl. Catal. A: Gen. 369 (2009) 15–26.
[30] L. Ji, J. Lin, H.C. Zeng, Chem. Mater. 13 (2001) 2403–2412.
[31] F. Millange, R.I. Walton, D. O'Hare, J. Mater. Chem. 10 (2000) 1713–1720.
[32] R.D. Shannon, Acta Crystallogr. A 32 (1976) 751–767.
[33] H. Yan, J. Lu, M. Wei, J. Ma, H. Li, J. He, D.G. Evans, X. Duan, J. Mol. Struct. Theochem. 866 (2008) 34–45.
[34] Y. Liu, F. Huang, J. Li, W. Weng, C. Luo, M. Wang, W. Xia, C. Huang, H. Wan, J. Catal. 256 (2008) 192–203.
[35] I. Balint, A. Miyazaki, K. Aika, J. Catal. 207 (2002) 66–75.
[36] P. Betancourt, A. Rives, R. Hubaut, C.E. Scott, J. Goldwasser, Appl. Catal. A: Gen. 170 (1998) 307–314.
[37] M. Fang, R.A. Sánchez-Delgado, J. Catal. 311 (2014) 357–368.
[38] J. Iwamoto, M. Itoh, Y. Kajita, M. Saito, K.-i. Machida, Catal. Commun. 8 (2007) 941–944.
[39] Q. Xu, J. Lin, X. Fu, D. Liao, Catal. Commun. 9 (2008) 1214–1218.
[40] Y.V. Larichev, B.L. Moroz, V.I. Zaikovskii, S.M. Yunusov, E.S. Kalyuzhnaya, V.B. Shur, V.I. Bukhtiyarov, J. Phys. Chem. C 111 (2007) 9427–9436.
[41] L. Chen, Y. Zhu, H. Zheng, C. Zhang, Y. Li, Appl. Catal. A: Gen. 411–412 (2012) 95–104.
[42] K. Hadjiivanov, J.C. Lavalley, J. Lamotte, F. Maugé, J. Saint-Just, M. Che, J. Catal. 176 (1998) 415–425.
[43] R.K. Brandt, M.R. Hughes, L.P. Bourget, K. Truszkowska, R.G. Greenler, Surf. Sci. 286 (1993) 15–25.
[44] J. Singh, J.A. van Bokhoven, Catal. Today 155 (2010) 199–205.
[45] Y.V. Larichev, J. Phys. Chem. C 112 (2008) 14776–14780.
[46] M.G. Cattania, F. Parmigiani, V. Ragaini, Surf. Sci. 211-212 (1989) 1097–1105.
[47] M.G. Mason, Phys. Rev. B 27 (1983) 748–762.
[48] Y.A. Ryndin, M.V. Stenin, A.I. Boronin, V.I. Bukhtiyarov, V.I. Zaikovskii, Appl. Catal. 54 (1989) 277–288.
[49] Y. Chen, K. Tomishige, K. Yokoyama, K. Fujimoto, J. Catal. 184 (1999) 479–490.
[50] K. Tomishige, Y. Chen, K. Fujimoto, J. Catal. 181 (1999) 91–103.
[51] D.P. Debecker, E.M. Gaigneaux, G. Busca, Chem. Eur. J. 15 (2009) 3920–3935.
[52] B. Rebours, d.l.C.J.B. d'Espinose, O. Clause, J. Am. Chem. Soc. 116 (1994) 1707–1717.
[53] M.F. Mark, W.F. Maier, J. Catal. 164 (1996) 122–130.
[54] C. Carrara, J. Múnera, E.A. Lombardo, L.M. Cornaglia, Top. Catal. 51 (2008) 98–106.
[55] P. Ferreira-Aparicio, I. Rodríguez-Ramos, J.A. Anderson, A. Guerrero-Ruiz, Appl. Catal. A: Gen. 202 (2000) 183–196.
[56] D. Liu, R. Lau, A. Borgna, Y. Yang, Appl. Catal. A: Gen. 358 (2009) 110–118.
[57] S. Natesakhawat, R.B. Watson, X. Wang, U.S. Ozkan, J. Catal. 234 (2005) 496–508.
[58] X. Lin, R. Li, M. Lu, C. Chen, D. Li, Y. Zhan, L. Jiang, Fuel 162 (2015) 271–280.
[59] Y. Gao, G. Bai, Y. Liang, G.C. Dunham, S.A. Chambers, J. Mater. Res. 12 (1997) 1844–1849.